CD74-NRG1 Fusions Are Oncogenic *In Vivo* and Induce Therapeutically Tractable ERBB2:ERBB3 Heterodimerization

Lisa Werr[1], Dennis Plenker[1,2,3], Marcel A. Dammert[1,2,3], Carina Lorenz[1,2,3], Johannes Brägelmann[1,2,3,4], Hannah L. Tumbrink[1,2,3], Sebastian Klein[5], Anna Schmitt[6], Reinhard Büttner[5], Thorsten Persigehl[7], Kevan M. Shokat[8,9], F. Thomas Wunderlich[3,10,11,12,13], Alison M. Schram[14,15], Martin Peifer[1,3], Martin L. Sos[1,2,3], H. Christian Reinhardt[16], and Roman K. Thomas[1,5,17]

ABSTRACT

NRG1 fusions are recurrent somatic genome alterations occurring across several tumor types, including invasive mucinous lung adenocarcinomas and pancreatic ductal adenocarcinomas and are potentially actionable genetic alterations in these cancers. We initially discovered *CD74-NRG1* as the first *NRG1* fusion in lung adenocarcinomas, and many additional fusion partners have since been identified. Here, we present the first CD74-NRG1 transgenic mouse model and provide evidence that ubiquitous expression of the CD74-NRG1 fusion protein *in vivo* leads to tumor development at high frequency. Furthermore, we show that ERBB2:ERBB3 heterodimerization is a mechanistic event in transformation by CD74-NRG1 binding physically to ERBB3 and that CD74-NRG1–expressing cells proliferate independent of supplemented NRG1 ligand. Thus, *NRG1* gene fusions are recurrent driver oncogenes that cause oncogene dependency. Consistent with these findings, patients with NRG1 fusion-positive cancers respond to therapy targeting the ERBB2:ERBB3 receptors.

Introduction

We previously discovered *NRG1* gene fusions in cancer; specifically, the *CD74-NRG1* gene fusion in invasive mucinous lung adenocarcinomas (IMA; ref. 1). Neuregulin 1 (NRG1) is an extracellular ligand of the ERBB3 receptor inducing pathway activation regulating plasticity in the central nervous system (2). The *CD74-NRG1* fusion is caused by an interchromosomal break and leads to ectopic expression of *NRG1* downstream of the *CD74* promoter. The gene fusion consists of a N-terminal membrane-bound CD74 portion and a C-terminal EGF-like domain of NRG1 that is localized at the outer cell membrane and has been shown to promote ERBB2-ERBB3 heterodimerization, triggering downstream survival and growth pathways, in particular PI3K/AKT/mTOR signaling (1, 3). Although a rare event, screening across larger cohorts of different cancer types has revealed that *NRG1* fusions occur in different types of solid tumors, including colorectal cancer, pancreatic ductal adenocarcinoma, cholangiocarcinoma, ovarian cancer, and sarcoma (3–6), thus raising the possibility that *NRG1*-rearranged carcinomas might be druggable with therapeutic strategies targeting ERBB-associated signaling pathways or the driving oncogene itself. NRG1 fusions are enriched in *KRAS* wild-type (wt) pancreatic cancer, and IMA of the lung and could represent genetic alterations for targeted therapies in these tumors (7, 8). Recent reports in cell line and xenograft models, in addition to early data in patients, confirm this assumption (9, 10). Clinical responses have been observed in patients treated with the pan-ERBB kinase inhibitor afatinib (11, 12), an anti-ERBB3 antibody (13), and the anti-ERBB2/ERBB3 bispecific antibody zenocutuzumab (14). Preliminary results from a phase I/II clinical trial of zenocutuzumab in NRG1 fusion-positive solid tumors revealed a response rate of 42% ($N = 5/12$), 25% ($N = 6/24$), and 22% ($N = 2/9$) in

[1]Department of Translational Genomics, Faculty of Medicine and University Hospital Cologne, University of Cologne, Cologne, Germany. [2]Molecular Pathology, Institute of Pathology, University Hospital of Cologne, Cologne, Germany. [3]Center for Molecular Medicine Cologne, University of Cologne, Cologne, Germany. [4]Mildred Scheel School of Oncology, Cologne, University Hospital Cologne, Medical Faculty, Cologne, Germany. [5]Institute of Pathology, Medical Faculty, University Hospital of Cologne, Cologne, Germany. [6]Department I of Internal Medicine, University Hospital of Cologne, Cologne, Germany. [7]Department of Radiology, Medical Faculty and University Hospital Cologne, University of Cologne, Cologne, Germany. [8]Howard Hughes Medical Institute, University of California San Francisco, San Francisco, California. [9]Department of Cellular and Molecular Pharmacology, University of California San Francisco, San Francisco, California. [10]Max Planck Institute for Metabolism Research, Cologne, Germany. [11]Institute for Genetics, University of Cologne, Cologne, Germany. [12]Cologne Excellence Cluster on Cellular Stress Responses in Aging-Associated Diseases (CECAD), Cologne, Germany. [13]Center for Endocrinology, Diabetes and Preventive Medicine (CEDP) Cologne, Cologne, Germany. [14]Department of Medicine, Memorial Sloan Kettering Cancer Center, New York, New York. [15]Weill Cornell Medical College, New York, New York. [16]Department of Hematology and Stem Cell Transplantation, University Hospital Essen, University Duisburg-Essen, German Cancer Consortium (DKTK partner site Essen), Essen, Germany. [17]DKFZ, German Cancer Research Center, German Cancer Consortium (DKTK), Heidelberg, Germany.

Note: Supplementary data for this article are available at Molecular Cancer Therapeutics Online (http://mct.aacrjournals.org/).

L. Werr and D. Plenker contributed equally to this article.

H.C. Reinhardt and R.K. Thomas contributed equally to this article.

Current address for L. Werr: Department of Experimental Pediatric Oncology, University of Cologne, Cologne, Germany; current address for D. Plenker, Loxo Oncology at Lilly, New York, New York, USA.

Corresponding Author: Roman K. Thomas, Department of Translational Genomics, Center of Integrated Oncology Cologne-Bonn, University of Cologne, Weyertal 115b, Cologne, 50931, Germany. E-mail: roman.thomas@uni-koeln.de

Mol Cancer Ther 2022;21:821–30

doi: 10.1158/1535-7163.MCT-21-0820

heavily pretreated pancreatic cancer, non–small cell lung cancer, and other solid tumors, respectively. These promising data suggest that genome-directed therapy targeting NRG1 fusions may become standard of care for patients harboring these alterations (14, 15).

Although available preclinical and clinical data support that NRG1 fusions are oncogenic drivers, it is still unknown whether these rearrangements are sufficient to induce oncogenesis *in vivo*. *In vitro*, lung adenocarcinoma cell lines expressing CD74-NRG1 exhibited enhanced ability to form colonies indicating that the *CD74-NRG1* gene fusion acts as an oncogene triggering cell growth (1). Patient-derived and cell-line xenograft models further support this assumption (11), albeit not by an intrinsic constitutive event in an immunocompetent *in vivo* model. Thus, the question remains unanswered, whether *NRG1* fusions themselves are sufficient to induce oncogenesis *in vivo*. Unlike oncogenic kinase fusions (such as those affecting ALK or ROS1), NRG1 itself is a ligand. Thus, the main caveat for interrogating the oncogenicity of NRG1 fusions is rooted in their dependency on coexpression of the ERBB3 receptor—which itself is kinase-dead and requires another kinase such as ERBB2 for heterodimerization and activation in cellular models. However, as the ectopic expression of wt ERBB2 has transforming potential on its own, suitable models with modest nontransforming levels of the ERBB2:ERBB3 receptors need to be used. In this article, we describe a solution to both limitations by employing a genetically engineered mouse model (GEMM) that ectopically expresses the CD74-NRG1 fusion and by use of a cellular model engineered to control dimerization of ERBB receptors (16).

Materials and Methods

Mice

The targeting vector depicted in **Fig. 1A** was constructed by using standard techniques. The targeting vector (Supplementary Fig. S1;

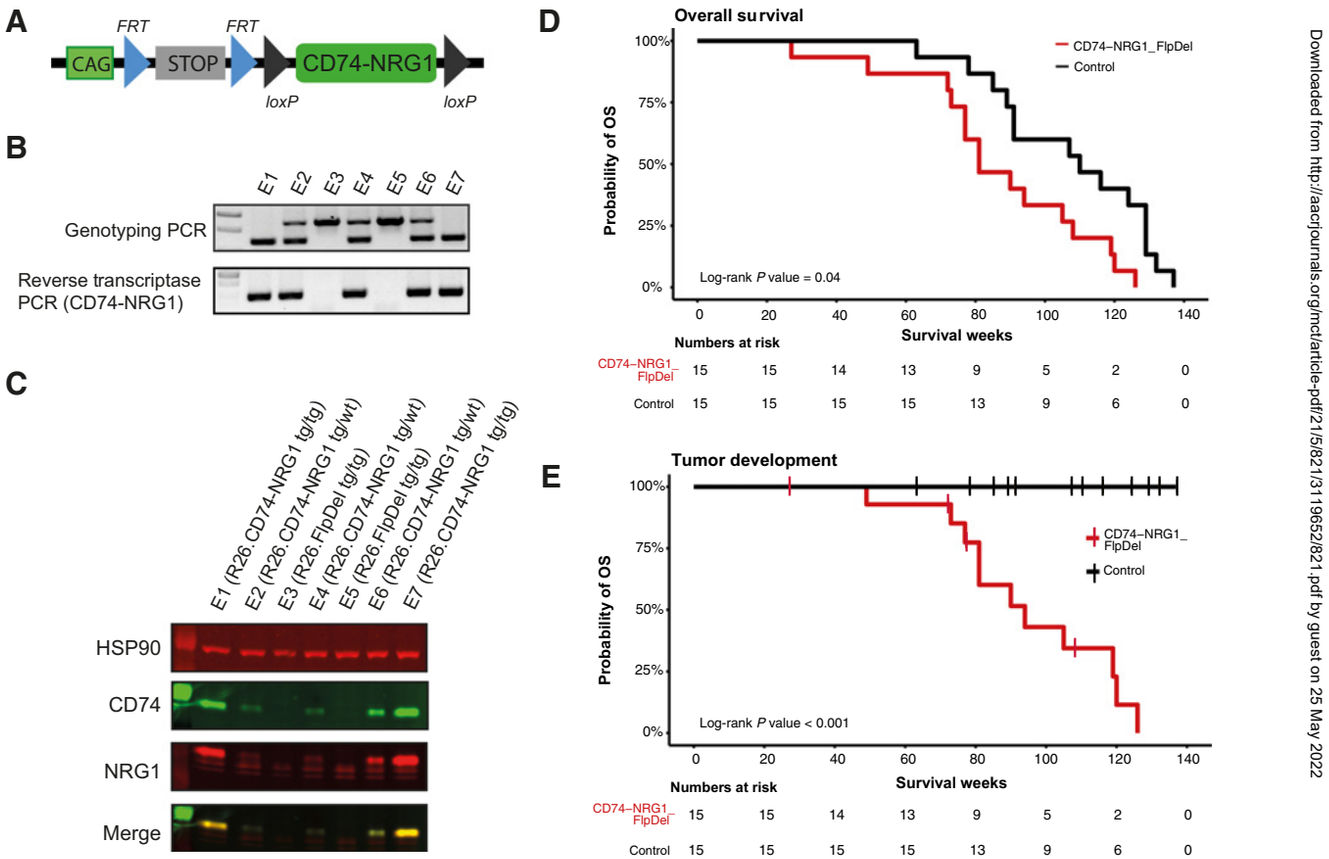

Figure 1.

Establishment of a CD74-NRG1 mouse model via homologous recombination at the ROSA26 locus. **A,** Representation of the primary targeting vector, where the CD74-NRG1 transgene (green) expression is driven by the CAG promotor but inactive due to a STOP cassette (gray). The stop cassette carries a kanamycin selection marker and is flanked by FRT sites (blue triangles), which provide target sites for the Flp recombinase that allow excision of the stop cassette and conditional activation of CD74-NRG1 transgene expression. **B,** Segregation and transcriptional activity of the CD74-NRG1 transgene in Rosa26$^{CD74\text{-}NRG1/Flp}$ mouse embryonic fibroblasts after Flp-mediated recombination. Genomic PCR differentiates a 570-bp ROSA26 wt amplicon and a 380-bp amplicon when the transgene is present; RT-PCR results in a 263-bp amplicon after excision of the stop cassette detects the CD74-NRG1 fusion transcript. **C,** Immunoblot of the same Rosa26$^{CD74\text{-}NRG1/Flp}$ mouse embryonic fibroblasts as in **B** to confirm protein expression. On top, a loading control stained with anti–HSP90. In the second panel: anti-CD74 staining in green, below an anti-NRG1 stain (red), and at the bottom, both protein determinants multiplexed (merged) resulting in a yellow signal. **D,** Kaplan–Meier curves illustrating the overall survival in the two transgenic mouse cohorts. Survival is significantly reduced only in the Rosa26$^{CD74\text{-}NRG1/Flp}$ cohort (red line) compared with either the control cohort (black line; $P = 0.04$). Rosa26$^{CD74\text{-}NRG1}$ mice were used as control, the CD74-NRG1 transgene is present in the Rosa26 locus but is not expressed without the Rosa26^{Flp} allele (stop cassette not excised in these mice). **E,** Alternative depiction of **D** when death in cohorts is recorded only in consequence of tumor development (log-rank P value < 0.001).

Supplementary Data S1) was generated (17) and transfected into the C57BL/6N Tac embryonic stem (ES) cell line. Targeted clones were isolated and correct integration was verified by Southern blotting. Correctly targeted ES cells were used to generate chimeras, which were backcrossed and examined for germ-line transmission. The following primers were used for genotyping: ROSA26 Forw (5′ AAAGTCGCTCTGAGTTGTTATC 3′), ROSA26 Rev (5′ GATATGAAGTACTGGGCTCTT 3′), and CAGGS Rev (5′ TGTCGCAAATTAACTGTGAATC 3′). Genotyping PCR was performed according to standard protocols resulting in a wt amplicon (570 bp) and a 380-bp amplicon for the transgenic allele.

This study was performed in accordance with FELASA recommendations. All animals were housed in a specific-pathogen-free facility, and animal breedings and experiments were approved by the local animal care committee and the relevant authorities (Landesamt für Natur, Umwelt und Verbraucherschutz Nordrhein-Westfalen, AZ: 84–02.04.2014.A146, 84–02.04.2016.A300). For overall survival analyses, animals that succumbed to disease or had to be killed due to satisfied termination criteria were recorded as events. Disease-specific survival animals that died from genotype-unrelated criteria (abnormal teeth, injuries inflicted by cage mates) were censored.

Generation of mouse embryonic fibroblasts

Mouse embryonic fibroblasts (MEFs) were generated using standard procedures. MEFs were cultured in DMEM supplemented with 1% penicillin/streptomycin, 10% FBS, 1% sodium pyruvate, and 1% nonessential amino acids.

cDNA synthesis

After RNA isolation, 1 μL of RNA was used for first-strand cDNA synthesis with the SuperScript III Reverse Transcriptase Kit (LifeTechnologies).

Reverse transcriptase PCR

The following primers were used to detect the CD74-NRG1 transcript: CD74-NRG1_Primer39 (CTTCCCGGAGAACCTGAGAC) and CD74-NRG1_Primer40 (ATCTCGAGGGGTTTGAAAG; ref. 17).

Immunoblot

Immunoblotting was performed as described previously (1). The following antibodies were used: anti-NRG1 β1 (R&D, AF-396-NA), anti-CD74 (Abcam, ab22604), anti-HSP90 (Cell Signaling Technology, No. 4877), anti-ERBB3 (Cell Signaling Technology, No. 4754), anti-phosphoERBB3 (Cell Signaling Technology, No. 4791), ERK1/2 (Cell Signaling Technology, No. 9102), anti-phosphoERK1/2 (Cell Signaling Technology, No. 9106), anti-AKT (Cell Signaling Technology, No. 9272), anti-phosphoAKT (Cell Signaling Technology, No. 9271), and β-actin-HRP (Santa Cruz Biotechnology, sc-47778). Secondary antibodies were IRDye800CW donkey anti-goat IgG (H+L; Licor, 925–32214), IRDye 680LT donkey anti-mouse IgG (H+L; Licor, 925–68022), and IRDye 800CW goat anti-rabbit IgG (H+L; Licor, 926–32211). Fluorescence detection was performed on Odyssey CLx Imaging System (Licor).

MRI

Mice were anesthetized with 2.5% isoflurane and scanned on a 3.0T MRI system (Igenia, Philips) with a small rodent solenoid coil (40-mm diameter, Philips Research Europe) with heating system. Axial T2-weighted images were acquired. Images were exported in DICOM format and analyzed using the Horos software.

IHC

Formalin-fixed and paraffin-embedded tissue from mice were cut into 4-μmol/L sections, H&E stained using standard techniques, and stained for Ki67 (Cellmarque, SP6, 1:1,000, 275R-16).

RNA sequencing

RNA was extracted using the RNeasy Mini Kit (Qiagen). 3′ UTR mRNA libraries were generated from total RNA (Lexogen QuantSeq Kit) according to the manufacturer's protocol and sequenced on Illumina HiSeq4000. Sequencing data were processed as described previously (18, 19). FASTQ files containing adapter-trimmed reads were to the mouse reference genome GRCm38 (mm10), respectively using the STAR aligner (20). Expression was quantified with RSEM (21). Adjusted expression fold-changes between samples were calculated from expression counts using DESeq2 (22). Data analysis was performed with R using the following packages: *AnnotationDbi*, *org.Mm.eg.db*, *fgsea*, *ggpubr*, and *stringr*.

Cell lines

NIH-3T3 cells were cultured in DMEM supplemented with 10% fetal calf serum (FCS) and 1% penicillin/streptomycin (PS). Parental Ba/F3 cells were cultured in RPMI supplemented with 10% FCS and 1% PS supplemented with 10 ng/mL IL3. Ba/F3 ERBB2YF/ ERBB3 wt cells were a kind gift from Kevan M. Shokat. Ba/F3 ERBB2YF/ ERBB3 wt cells were cultured in RPMI (Gibco) supplemented with 10% FCS and 1% PS supplemented with 6.25 ng/mL recombinant human NRG1. Human Neuregulin-1 (hNRG-1) from Cell Signaling Technology No. 5218 was used for the cell culture, this recombinant human NRG-1 Thr176-Lys238 (Accession No. NP_001153480) was produced in *Escherichia coli* cells. NP_001153480 is the NCBI accession number for isoform HRG-beta2b. The cell lines have been authenticated via genotyping (SNP 6.0; Affymetrix) or verified by STR profiling at the Institute for Forensic Medicine of the University Hospital of Cologne. All cells were grown in a humidified incubator at 37°C and 5% CO_2 and tested regularly for mycoplasma infection.

Transduction

Cells were seeded at 50% confluence. Viral supernatant (80% of final volume) and 20% fresh growth media were mixed and 8-μg/mL polybrene (Santa Cruz Biotechnology) was added to the cells. The viral supernatant was kept on the cells for 24 to 48 hours to allow proper infection of cells. After 48 hours of the initial transduction, the media was exchanged with complete growth media containing an appropriate amount of antibiotics (3-μg/mL puromycin, 800-μg/mL hygromycin, or 800-μg/mL geneticin, LifeTechnologies). Antibiotics were exchanged every 4 days until control cells (nontransduced cells) were negatively selected.

Cell counting

A total of 30,000 cells were plated in 6-well plates (day 0). After 24 hours, at day 4 and day 8 duplicated were counted by using a Z2 particle counter (Beckman Coulter). Graphs were plotted with GraphPad Prism.

Co-immunoprecipitation

Four hundred micrograms of protein lysate was incubated with agarose beads (Santa Cruz Biotechnology) for 1 hour at 4°C following centrifugation at 1,000 × *g* at 4°C for 5 minutes. The precleared lysates were incubated overnight with CD74 or ERBB3 antibody at 4°C. The following morning, the antibodies were immunoprecipitated with

Protein A-agarose (mouse; CD74) or Protein G-PLUS agarose beads (rabbit, ERBB3), and extensively washed with PBS. The beads were resuspended in 30-μL Laemmli buffer and boiled for 5 minutes. The supernatant was used straight to load a polyacrylamide gel (4%–12%; NOVEX) following standard procedures.

Cell viability assays

A total of 3,000 cells per well in triplicates were treated for 96 hours. Viability was measured by CellTiter-Glo assay (Promega, catalog No. G7572). Luminescence was measured on a Tecan Infinite M1000 pro. The values were normalized to untreated controls on each plate.

Data availability statement

The data generated in this study are publicly available in Gene Expression Omnibus (GEO) at GSE184004. Further information and request for data, resources, and reagents should be directed to and will be fulfilled upon reasonable request by the lead contact, Roman Thomas (roman.thomas@uni-koeln.de).

Results

To test the potential oncogenicity of the human *CD74-NRG1* fusion [first six exons of the human *CD74*; NM_004355 and exon 4 and 5 (exon 10a and 12b) of human *NRG1*; NM_001160005; ref. 1] *in vivo*, we created a conditional *Rosa26 CD74-NRG1* knock-in mouse strain ($Rosa26^{FSF.CD74\text{-}NRG1}$). For the generation of this mouse model, the human *CD74-NRG1* cDNA obtained from the first discovered CD74-NRG1 patient sample was used (1). In this index tumor sample, only the expression of the isoform NM_001160005 (NRG1 III-β3) was highly elevated, all other NRG1 isoforms were not expressed (1). To evaluate the effect of expression of this specific fusion protein and isoform, the human cDNA was used to generate the targeting vector. To this end, the STOP-EGFP-ROSA CAG targeting vector was modified such that a FRT-flanked STOP cassette prevents expression of the *CD74-NRG1* transgene from the CAG (cytomegalovirus early enhancer/chicken β actin) promoter (**Fig. 1A**; ref. 17). Flp-recombinase-mediated excision of the FRT flanked Stop cassette leads to CD74-NRG1 expression in transgenic mice. To test this newly generated mouse model, we crossed $Rosa26^{FSF.CD74\text{-}NRG1}$mice with an established Flp deleter strain ($Rosa26^{Flp}$), which results in early embryonic excision of the FRT-flanked stop cassette and subsequent ubiquitous expression of the CD74-NRG1 fusion in all tissues of the resulting $Rosa26^{FSF.CD74\text{-}NRG1/Flp}$mice (23). To generate murine embryonic fibroblasts (MEFs) out of these $Rosa26^{FSF.CD74\text{-}NRG1/Flp}$ mice, $Rosa26^{FSF.CD74\text{-}NRG1/Flp}$mice carrying the CD74-NRG1 transgene as well as the Flp deleter allele were mated. Because of the Flp allele, the stop cassette can be excised and in the offspring embryos homozygous ($Rosa26^{FSF.CD74\text{-}NRG1/FSF.CD74\text{-}NRG1}$) and heterozygous ($Rosa26^{FSF.CD74\text{-}NRG1/Flp}$) for the transgene, as well as CD74-NRG1 negative embryos ($Rosa26^{Flp/Flp}$) were used for MEF generation. Genotyping with primers that discriminate between a larger wt and a smaller transgenic amplicon revealed two homozygous and three heterozygous embryos, as well as two CD74-NRG1 negative embryos (**Fig. 1B**). Confirming our overall strategy, a PCR product was detectable only in MEFs carrying the *CD74-NRG1* transgene by employing a reverse transcriptase PCR with *CD74-NRG1* spanning primers (**Fig. 1B**; Supplementary Fig. S1). Furthermore, we confirmed protein expression of the fusion in those MEFs generated out of $Rosa26^{FSF.CD74\text{-}NRG1/Flp}$ mice by immunoblotting using antibodies against CD74 and NRG1 (**Fig. 1C**). As shown in **Fig. 1C**, we detected the fusion at the expected size with both antibodies. A merged image (**Fig. 1C**) shows an overlay of both signals with a molecular weight of ∼35 kDa. The observed molecular weight also confirmed expression of the fusion protein, as the endogenous murine NRG1 is expected to have a molecular weight of 44 kDa, and the endogenous murine CD74 protein has an expected molecular weight of 24 kDa. CD74-NRG1 protein levels correlated with the genotype of the murine embryos: wt MEFs exhibited no CD74-NRG1 protein expression, whereas heterozygous and homozygous cells had varying levels of protein expression with higher levels in MEFs homozygous for the transgene (**Fig. 1C**). Finally, transcriptome sequencing of transgenic MEFs confirmed that that Nrg1 was the most differentially expressed gene relative to wt MEFs (Supplementary Figs. S2 and S3).

As our results in MEFs confirmed expression of the desired transgene after Flp-mediated recombination, we employed the mouse model to interrogate the potential oncogenicity of the CD74-NRG1 fusion *in vivo*. To test the effects of CD74-NRG1 fusion expression, we mated $Rosa26^{FSF.CD74\text{-}NRG1}$mice with the $Rosa26^{Flp}$ deleter strain (23) that were previously described and were already used for the generation of the MEFs ($N = 15$). The same number of unflipped $Rosa26^{FSF.CD74\text{-}NRG1}$(CD74-NRG1 transgene present in the Rosa26 locus, but not expressed) animals served as control. In 11 of 15 $Rosa26^{FSF.CD74\text{-}NRG1/Flp}$ progeny, we observed tumor development by MRI and significantly reduced overall survival in comparison the untreated control cohort (**Fig. 1D**, log-rank $P = 0.04$). This is especially evident in disease-specific survival in **Fig. 1E**, when only tumor development–related death was recorded as an event (red curve), whereas other genotype-unrelated deaths were censored.

In the 11 tumor-bearing mice of the $Rosa26^{FSF.CD74\text{-}NRG1/Flp}$ cohort, tumors were predominantly found at different locations in the subcutis (eight of 11 mice). One of these mice had developed two subcutaneous tumor lesions. MRI revealed fuzzy-edged, oval-shaped tumors with inhomogeneous internal signal (T1 intermediate, T2 hyperintense without signal suppression in the fat-saturated sequences, **Fig. 2A**) that did not invade surrounding tissues. Histologic examination revealed malignant spindle cell neoplasia with neurogenic or myogenic differentiation (**Fig. 2B**), a pattern typically observed in subcutaneous sarcomas. Ki67 staining, a criterium for malignancy, was also positive (**Fig. 2C**). In addition to the predominant subcutaneous tumors, we observed liver tumors in three mice, which developed in two animals with sarcomas. None of the liver tumors shared the histology of the subcutaneous tumors, thus arguing against metastasis. Two mice developed an intraperitoneal tumor with unclear histology in the absence of a detectable subcutaneous tumor. We next sought to characterize the different tumors further by transcriptome sequencing comparing isolated tumor tissue to different normal tissue samples from individual animals. Principal component analysis indicated that normal samples cluster in a tissue-specific manner, and sarcoma samples form a distinct cluster (**Fig. 2D**). According to hierarchical cluster analysis of 10 tumors that arose in eight individual mice, subcutaneous tumors ($n = 7$) represented a discrete and isolated cluster and liver tumors ($n = 3$) co-clustered with the corresponding normal liver tissue (Supplementary Fig. S4A). The presence of tumors in 11 of 15 $Rosa26^{FSF.CD74\text{-}NRG1/Flp}$ mice and their complete absence in the control cohort indicates that expression of the *CD74-NRG1* transgene is sufficient to induce tumorigenesis *in vivo* and is the critical oncogenic event. As the histologic examination of the liver or intraperitoneal tumors remained inconclusive compared with malignant spindle cell neoplasia in eight of 15 the $Rosa26^{FSF.CD74\text{-}NRG1/Flp}$ mice, we conducted further analyses in these tumors.

CD74-NRG1 fusions had originally been detected in invasive mucinous lung adenocarcinomas (1). We therefore compared the expression data of the subcutaneous tumors arising in *CD74-NRG1* transgenic mice with those of normal lung tissue (Supplementary Figs. S4B and S4C). In addition, based on histology and myogenic differentiation of sarcomas, we also compared the subcutaneous tumors to normal muscle tissue. Comparison of the native, that is, murine *Nrg1* transcript levels between the subcutaneous tumors and lung or muscle tissue showed no significant differences (Supplementary Fig. S4B). This observation is in line with the ubiquitous expression of the *CD74-NRG1* transgene, as 3′ mRNA sequencing cannot discriminate between transcripts derived from the native *Nrg1* gene and the *CD74-NRG1* transgene. As we did not observe any lung tumors, it seems as if the expression of the CD74-NRG1 fusion protein is not alone crucial for tumorigenesis. Therefore, we assumed that co-expression of ERBB3 (kinase-dead) and another ERBB receptor is required. In support of this notion, we found high transcript levels of *Erbb2* and *Erbb3* in the subcutaneous mouse sarcomas relative to muscle normal tissue (**Fig. 2E**; Supplementary Fig. S4C). Although we failed to show that the *CD74-NRG1* fusion is sufficient to act as an oncogene in the lung, the subcutaneous sarcomas in our model show that the fusion is oncogenic *in vivo*, which is accompanied by elevated transcript levels of *Erbb2* and *Erbb3*.

The correlation between *CD74-NRG1*–induced sarcomas in our mouse model and elevated *Erbb2* and *Erbb3* transcript levels prompted us to test this interdependent relationship *in vitro*. We therefore used genetically engineered murine Ba/F3 cells that express a mutant variant of ERBB2. Replacement of the C-terminal tyrosine by phenylalanine (16) results in a mutated ERBB2-YF receptor that is defective in homodimerization. When co-expressed with ERBB3 in BaF3 *ERBB2-YF/ERBB3* wt cells, the formation of active ERBB2-YF/ERBB3 heterodimers is dependent on the availability of an activating extracellular ligand such as NRG1. For proliferation, BaF3 *ERBB2-YF/ERBB3* wt cells are fully dependent on the presence of exogenously added recombinant NRG1 in the cell culture media (**Fig. 3A**; ref. 16). However, upon ectopic expression of CD74-NRG1, we observed that BaF3 *ERBB2-YF/ERBB3* wt cells became independent of exogenously added NRG1 (**Fig. 3A**). The proliferation of BaF3 *ERBB2-YF/ERBB3* wt *CD74-NRG1* cells in the absence of exogenously added NRG1 is therefore due to autocrine or paracrine presentation of the CD74-NRG1 fusion protein on the cell surface, thus promoting the formation of ERBB2:ERBB3 heterodimers and subsequent activation of downstream signaling. Additional support for this conclusion came from the use of small-molecule ERBB kinase inhibitors, which effectively reduced proliferation of BaF3 *ERBB2-YF/ERBB3* wt cells that express the CD74-NRG1 fusion (**Fig. 3B–D**). The small-molecule kinase inhibitor, afatinib, has the strongest antiproliferative effect in this model (**Fig. 3B**). Furthermore, lapatinib that inhibits EGFR and ERBB2 (**Fig. 3C**), as well as Compound 3 (**Fig. 3D**; Supplementary Fig. S5; ref. 16) that inhibits active heterodimers of ERBB2 and ERBB3, both exhibited strong antiproliferative effects in BaF3 *ERBB2-YF/ERBB3* wt *CD74-NRG1* cells, which are independent of exogenously added recombinant NRG1. Thus, ectopically expressed CD74-NRG1 can compensate for exogenous addition of NRG1, thereby creating a therapeutically tractable dependency on the associated ERBB2:ERBB3 signaling. Consistent with this notion, we found that BaF3 *ERBB2-YF/ERBB3* wt cells transduced with empty vector and BaF3 *ERBB2-YF/ERBB3* wt expressing CD74-NRG1 cells exhibited a dose-dependent reduction of pAKT and pERK levels under treatment with 10- and 100-nmol/L afatinib or compound 3 (**Fig. 3E**).

To further investigate the potential of CD74-NRG1–dependent activation of the ERBB3 receptor, ERBB2 and ERBB3 were co-expressed with individual selection markers in NIH-3T3 cells either with empty vector control, CD74-NRG1, or a truncated version of CD74-NRG1 lacking the EGF-like activation domain (CD74-NRG1_del; stop codon introduced after aa230, before the EGF-like domain starts, Supplementary Fig. S6). In a proof-of-concept experiment ERBB2, ERBB3, and the CD74-NRG1 constructs were co-expressed in all cells (schematic representation in **Fig. 4A**). Co-immunoprecipitation with anti-ERBB3 (**Fig. 4B**) and anti-CD74 (**Fig. 4C**) antibodies was performed with cells overexpressing different combinations of ERBB2, ERBB3, and CD74-NRG1/CD74-NRG1_del. Only full-length CD74-NRG1 fusion (including the EGF-like domain) could be captured in the ERBB3-co-immunoprecipitation proofing the EGF-like domain binding to ERBB3 (**Fig. 4B**). Vice versa, in the CD74 co-immunoprecipitation, we could detect the full-length and truncated version of CD74-NRG1 with an NRG1 antibody, but ERBB3 could be only captured when ERBB3 and full-length CD74-NRG1 were co-expressed. These co-immunoprecipitation experiments therefore confirm the ability of full-length CD74-NRG1 to interact with ERBB3. To further determine if this interaction can happen via paracrine signaling of CD74-NRG1 and ERBB3—that is, between neighboring cells—we conducted a complementary experiment, in which we mixed NIH-3T3 cells overexpressing ERBB2 and ERBB3 with cells overexpressing CD74-NRG1 or CD74-NRG1_del and incubated the cells overnight (**Fig. 4D**). ERBB3 co-immunoprecipitations (**Fig. 4E**) and CD74-NRG1 co-immunoprecipitations confirmed the interaction of full-length CD74-NRG1 and ERBB3 indicating as well paracrine signaling mechanism. Because the immunoblots of CD74-NRG1 showed a stronger signal when the fusion protein was co-expressed in the same cells with ERBB2:ERBB3, our results indicate that the CD74-NRG1 fusion can also signal in an autocrine manner (compare **Fig. 4B** and **C** and **Fig. 4E** and **F**).

In summary, these experiments provide evidence that CD74-NRG1 on the cell surface can bind to ERBB3 in autocrine and paracrine fashion, resulting in heterodimerization of ERBB2 and ERBB3 and activation of downstream pathways important for survival and cell growth.

Discussion

Here, we show that ubiquitous expression of CD74-NRG1 in a GEMM causes tumor formation. Thus, *CD74-NRG1* rearrangements are oncogenic *in vivo* and can drive tumorigenesis. Because *NRG1* rearrangements are found in tumors that are otherwise hard or impossible to treat (i.e., invasive mucinous lung adenocarcinoma, pancreatic cancer), our observation provides mechanistic support for therapeutic strategies targeting the associated oncogenic signaling. We did not observe the expected development of lung tumors or other cancers (e.g., pancreatic adenocarcinoma) typically associated with NRG1 fusions. Further experimental *in vivo* models are therefore required to clarify the specific role of NRG1 fusions in these tumor types. One limitation of our study is the expression of the cDNA construct of *CD74-NRG1* instead of the full genomic locus. In CD74-NRG1 positive lung adenocarcinomas, transcription is under the control of the human *CD74* promoter (1). In the mouse model examined, the CD74-NRG1 fusion protein was expressed ubiquitously under the control of the CAG promoter after the construct had been integrated into the ROSA26 locus. Regulation of expression could therefore be different in tumor cells with NRG1 fusions resulting from chromosomal rearrangements. The lack of regulatory or splicing sites

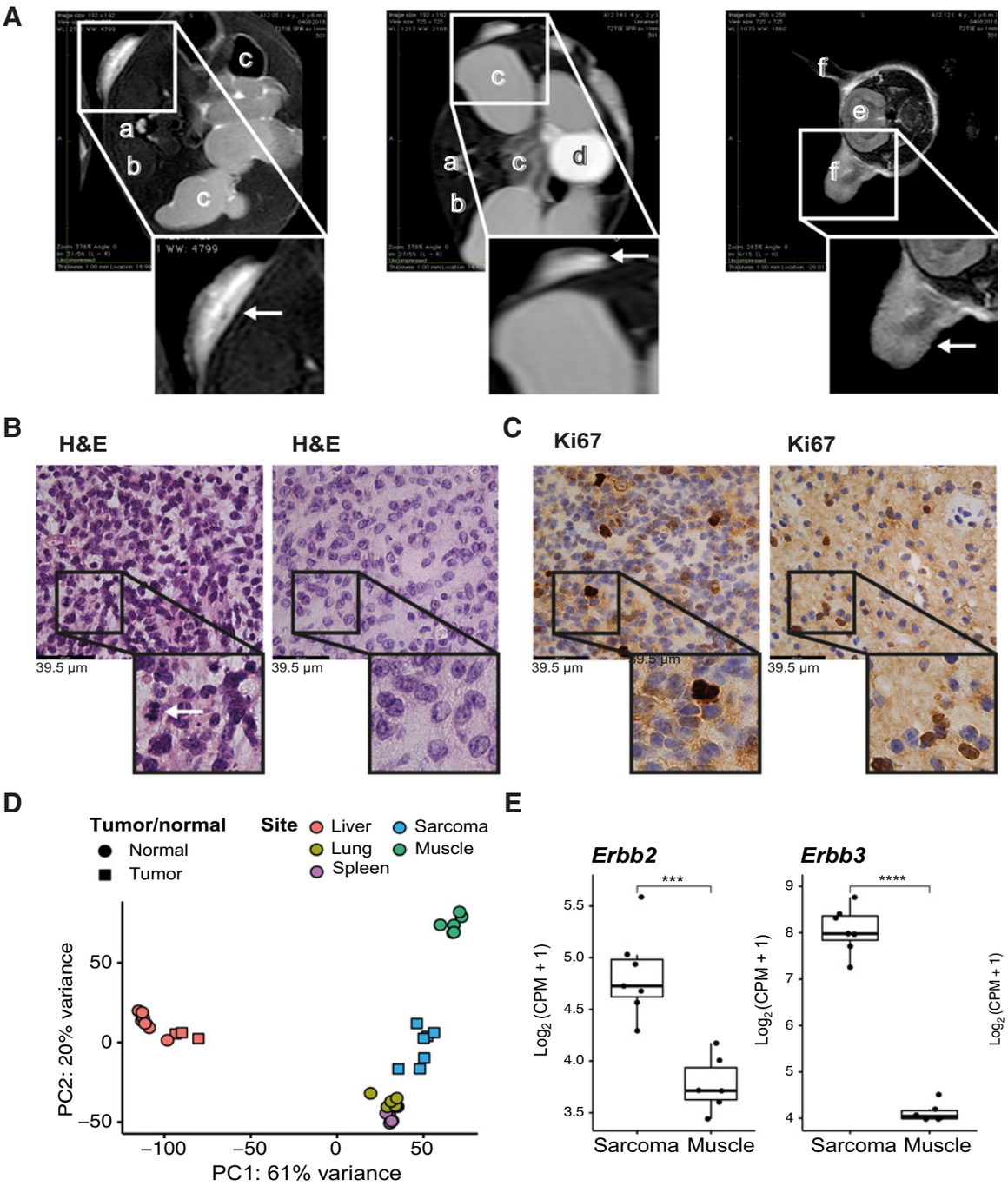

Figure 2.

Subcutaneous tumors in Rosa26$^{CD74\text{-}NRG1/Flp}$ mice and characterization. **A,** MRI scans of representative tumors in Rosa26$^{CD74\text{-}NRG1/Flp}$ mice scanned on a 3.0T MRI system in a monthly interval. Letters indicate names of organs/tissues (a, spine; b, paravertebral muscle tissue; c, intestine; d, urinary bladder; e, brain; f, ear). Axial T2-weighted images show subcutaneous tumors in three different mice at different locations. The boxes below each primary picture represent magnifications where arrows point to subcutaneous tumor tissue. **B,** H&E staining of two different subcutaneous tumors from independent Rosa26$^{CD74\text{-}NRG1/Flp}$ mice, representative areas are boxed and magnified fourfold below. The white arrow points to a mitotic cell. **C,** Ki67 staining results of the same tumors as in **B** and a fourfold magnification of representative areas. Scale bars at the bottom left in **B** and **C** represent 39,5 µmol/L. **D,** Principal component analysis (PCA) of 3′RNA-Seq results comparing normal and tumor tissue of Rosa26$^{CD74\text{-}NRG1/Flp}$ mice. Variance stabilizing transformation (VST) was performed on the 1,000 most variably transcribed genes. Each square indicates a tumor sample, each dot represents a normal tissue sample. First principal component (PC1) on the *x*-axis explains 61% of the variance and is plotted against second principle component (PC2) on the *y*-axis that accounts for 20% variance among samples. Colors indicate tissue origin of the sample (red = liver, yellow = lung, green = muscle, blue = subcutaneous sarcoma, purple = spleen). **E,** Transcript levels of *Erbb2* and *Erbb3* estimated by 3′RNA-Seq in sarcoma tissue compared normal muscle tissue of Rosa26$^{CD74\text{-}NRG1/Flp}$ mice are plotted for seven animals. Dots on the *y*-axis represent gene expression values [log2 (CPM+1)].

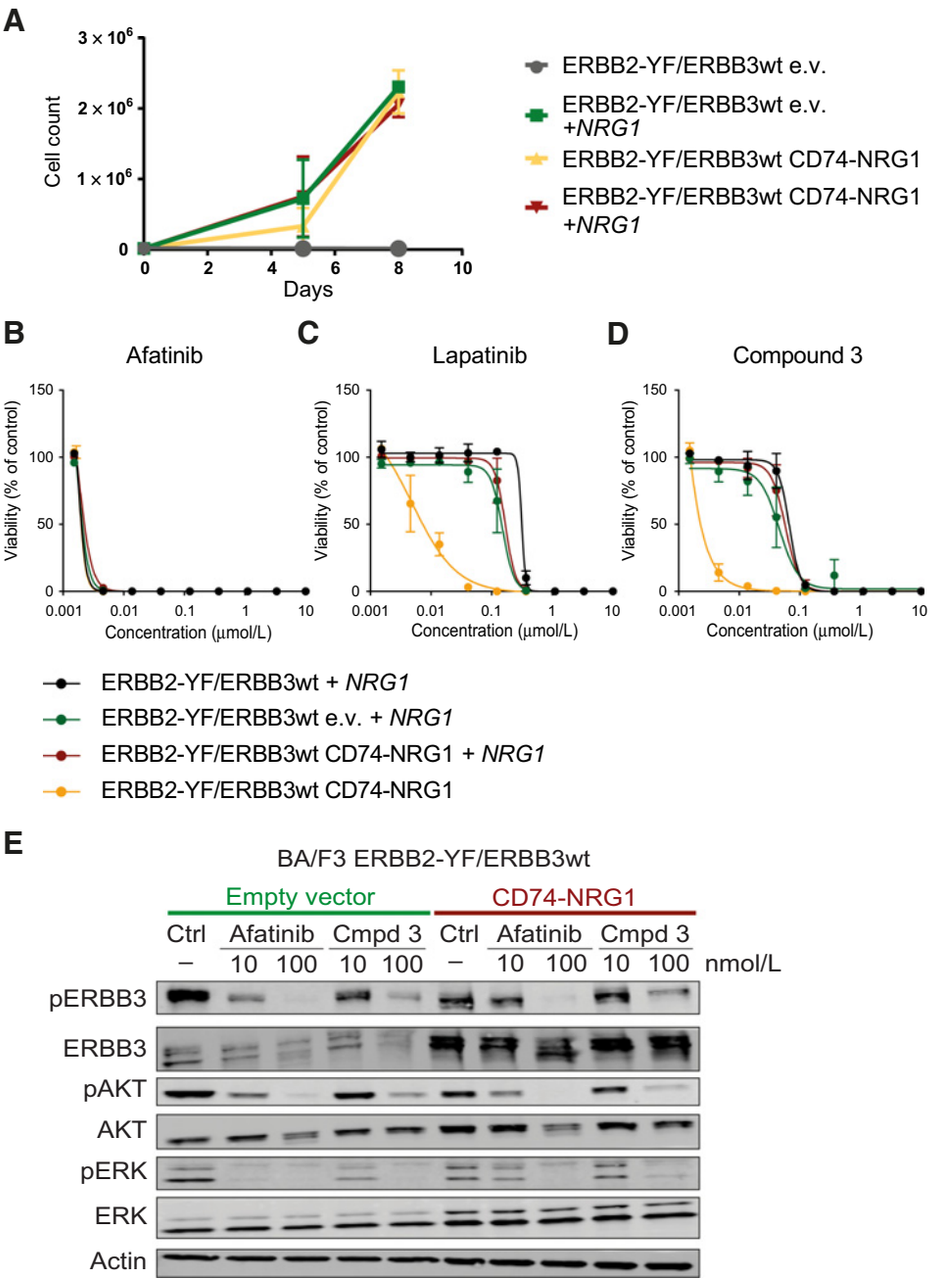

Figure 3.

CD74-NRG1 expressing cells are sensitive to ERBB2 and ERBB3 inhibitors. **A,** Proliferation of *BaF3 ERBB2 2YF/ERBB3 wt* cells over time after transduction with pBabe-hygro-CD74-NRG1 or pBabe-hygro empty vector (time in days plotted on the *x*-axis, cell count in cells/mL on the *y*-axis). The color code to the left of the graph indicates whether the pBabe-hygro empty vector control (e.v.) or the pBabe-hygro-CD74-NRG1 vector were used for cell transduction and whether recombinant NRG1 was supplemented or not. Note that in the absence of NRG1 *BaF3 ERBB2 2YF/ERBB3 wt* cell proliferation strictly depends on NRG1 (compare green squares to dark gray dots), whereas CD74-NRG1 expression of (ERBB2-YF/ERBB3 wt CD74-NRG1) releases this requirement (compare yellow to red triangle curve). **B–D,** Viability screening of *BaF3 ERBB2 2YF/ERBB3 wt* cells treated with afatinib (**B**), lapatinib (**C**), and Compound 3 (**D**) for 96 hours ($n = 3$). Each graph compares cell viability in nontransduced *BaF3 ERBB2 2YF/ERBB3 wt* cells (gray), to cells transduced with the empty pBabe-hygro (green) or the pBabe-hygro-CD74-NRG1 vector (red and yellow). Note that CD74-NRG1 cells (yellow curves) proliferate independently of NRG1, whereas BaF3 ERBB2 2YF/ERBB3 wt cells not expressing CD74-NRG1 require exogenous NRG1 supply. In each experimental set-up, every inhibitor efficiently reduces cell proliferation in pBabe-hygro-CD74-NRG1 transduced cells that are not supplemented with NRG1. **E,** Immunoblot analysis of *BaF3 ERBB2 2YF/ERBB3 wt* transduced with either empty vector or a construct encoding CD74-NRG1 were treated with afatinib and Compound 3 for effects on downstream activation of HER3. Cells were treated for 6 hours. Inhibitor concentrations are depicted on the top, antibodies used to evaluate downstream activation of ERBB3 are shown on the left side. Actin was used as a loading control.

and other ncRNAs from the cDNA construct might explain the formation of sarcomas instead of adenocarcinomas, and therefore further research is needed to understand these differences. Furthermore, we are only addressing with this work the CD74-NRG1 fusion, which will likely translate into other NRG1 fusions that involve signaling through the extracellular part of NRG1 containing the EGF-like domain, however, not the NRG1 fusions that contain a cytoplasmic portion of NRG1 that might use a different mechanism for their oncogenic contribution.

In addition, the big family of Neuregulin with more than 30 isoforms and isoform-specific functions are challenging for the oncogenic function of Neuregulins (2, 24). Although NRG1 type II itself consists of nine isoforms with some lacking the EGF-like domain and different cytoplasmic tails, nearly all so far described NRG1 fusions only contain the extracellular domain of NRG1 and retain the EGF-like domain that is essential for its oncogenic function, whereas the 5′ fusion partner acts as a scaffold for expression and its localization. In line with these clinical observations, recombinant NRG1 can make cancer cell lines driven by other oncogenes such as ERBB2, FGFR, MET, EML4-ALK, or BRAF resistant when ERBB3 is expressed (25).

Because NRG1 containing the EGF-like domain signals via surface receptors such as ERBB2 and ERBB3, suitable surface receptors are probably crucial. Critical parameters are therefore the respective expression level in different tissue types or, in the case of obligatory

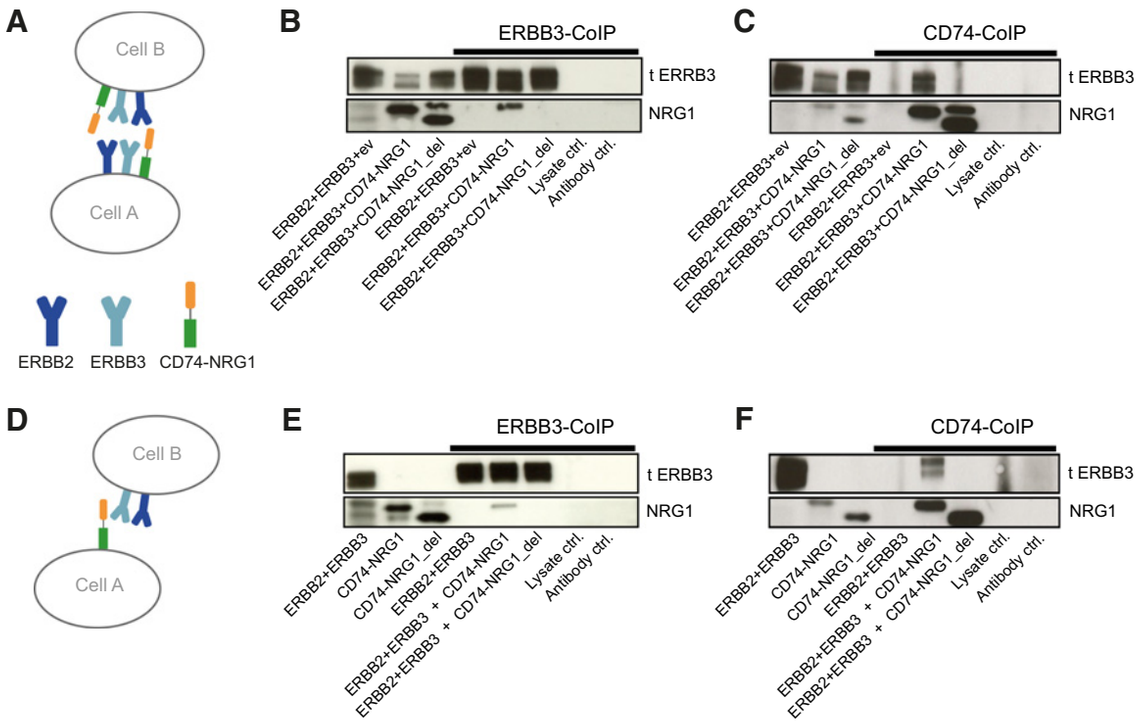

Figure 4.

Evidence for autocrine and paracrine CD74-NRG1 signaling. **A,** Schematic representation of cells overexpressing ERBB2, ERBB3, and CD74-NRG1 with different resistance cassettes in all individual cells. (paracrine and autocrine interaction). **B** and **C,** Immunoblots of ERBB3 (**B**) and CD74 (**C**) co-immunoprecipitations with lysates from NIH-3T3 cells overexpressing combinations of ERBB2, ERBB3, CD74-NRG1, CD74-NRG1_del, or empty vector (ev). **D,** An experiment in which cells are mixed 1:1 overexpressing ERBB2 and ERBB3 and cells overexpressing CD74-NRG1 with different resistance cassettes in all individual cells (paracrine interaction only). **E** and **F,** Immunoblots of ERBB3 (**B**) and CD74 (**C**) co-immunoprecipitations with lysates from 1:1 mixed NIH-3T3 cells overexpressing ERBB2 and ERBB3 and cells overexpressing CD74-NRG1 or CD74-NRG1_del.

heterodimers, the availability of the respective partners. Both could explain the different effects of CD74-NRG1 expression, for example, the formation of sarcomas in contrast to lung carcinomas in the mouse model.

To better mimic the clinical state of NRG1 fusion-positive aggressive growing tumors, like lung adenocarcinoma (1) and pancreatic ductal adenocarcinomas (8), tissue-specific expression of the transgene in combination with other genetic alterations such as knockout of tumor suppressor genes would be an option.

Mechanistically, we provide evidence that the CD74-NRG1 fusion activates ERBB2:ERBB3 heterodimer formation that is required for cellular proliferation and survival. Thus, approaches that disrupt ERBB2:ERBB3 heterodimerization are particularly promising for therapies of NRG1-rearranged tumors. Accordingly, the mAb, zenocutuzumab, which blocks NRG1-dependent ERBB2:ERBB3 complex formation has been shown to induce tumor shrinkage in NRG1-rearranged cancers in early clinical trials. We also show that both paracrine and autocrine receptor activation followed by downstream signaling can play a role in the transformation process elicited by CD74-NRG1. Our data employing Ba/F3 *ERBB2 2YF/ERBB3* wt cells highlight the interdependence between NRG1 fusions and ERBB receptor family members and thus support our previous observations made in established lung cancer cell lines. Our previous finding of enhanced ERBB2 and ERBB3 gene expression in *NRG1*-rearranged carcinomas further supports this notion (1). Finally, co-immunoprecipitation experiments indicate that CD74-NRG1 can bind to ERBB3 receptors of neighboring cells in a paracrine fashion but seems to be more effective activating ERBB2:ERBB3 downstream signaling when occurring via autocrine signaling. However, NRG1 can be secreted and act as an autocrine growth factor in some cancer cells (26). As we investigated the CD74-NRG1 fusion with a membrane-bound CD74 portion and a C-terminal EGF-like domain of NRG1 localized at the outer cell membrane and lacking the shedding site, it was important to evaluate the effect of expression on surrounding cells. Understanding if paracrine is sufficient for its oncogenicity might be the basis of future studies involving single-cell sequencing. These studies might be able to answer as well the question for the cell of origin of *NRG1*-rearranged tumors.

In summary, our findings provide formal proof that the CD74-NRG1 fusion is a *bona fide* oncogene *in vivo* and establishes NRG1-dependent ERBB2:ERBB3 heterodimerization and subsequent signaling as key mechanisms involved in transformation by the fusion. Thus, our data provide a mechanistic explanation for the clinical activity of therapeutic approaches targeting ERBB2:ERBB3 heterodimerization and downstream signaling and provide a methodologic framework for testing of novel therapies in NRG1-rearranged cancers.

Authors' Disclosures

L. Werr reports other support from Köln Fortune program and grants from German Research Foundation during the conduct of the study. D. Plenker reports a patent for "NRG1 fusion genes in cancer"—US10208354B2—issued. J. Brägelmann reports grants

from Deutsche Krebshilfe during the conduct of the study. H.L. Tumbrink reports personal fees from PearlRiver Bio (now a Centessa Pharmaceuticals company) outside the submitted work. R. Büttner reports personal fees and other support from Amgen, MSD, BMS, AbbVie, Merck-Serono, and Novartis outside the submitted work and reports a grant from the German Cancer Aid. K.M. Shokat reports personal fees and other support from Erasca during the conduct of the study; personal fees from Roche and Black Diamond outside the submitted work; and has a patent for Compound 3 (covered by a UCSF filed patent pending); and reports stock and/or cash compensation with the following companies: Apertor, BioTheryX, BridGene Biosciences, Denali Therapeutics, eFFECTOR Therapeutics, Erasca, G Protein Therapeutics, Genentech/Roche, Ikena, Initial Therapeutics Janssen Pharmaceuticals, Kumquat Biosciences, Kura Oncology, Merck, Mitokinin, Nested, Nextech, Radd Pharma, Turning Point, Type6 Therapeutics, and Wellspring Biosciences (Araxes Pharma). A.M. Schram reports other support from Merus during the conduct of the study; other support from AstraZeneca, ArQule, BeiGene/Springworks, Black Diamond Therapeutics, Elevation Oncology, Kura Oncology, Eli Lilly, Northern Biologics, Pfizer, PMV Pharma, Relay Therapeutics, Repare Therapeutics, Revolution Medicine, and Surface Oncology outside the submitted work. M.L. Sos reports grants, personal fees, and other support from PearRiver Bio (part of Centessa Pharmaceuticals) outside the submitted work. H.C. Reinhardt reports personal fees from AbbVie, Novartis, and BMS and grants from Gilead and AstraZeneca outside the submitted work. R.K. Thomas reports grants from BMBF Federal Ministry of education and research during the conduct of the study; personal fees and other support from NEO New Oncology (now part of Siemens Healthcare), PearlRiver Bio (now part of Centessa Pharmaceuticals), and Epiphanes Inc.; grants from Roche outside the submitted work; and has a patent for "Novel fusion genes in lung cancer" (WO 2015/018918 A1) issued. No disclosures were reported by the other authors.

Authors' Contributions

L. Werr: Conceptualization, formal analysis, validation, investigation, visualization, methodology, writing–original draft, writing–review and editing. **D. Plenker:** Conceptualization, formal analysis, validation, investigation, visualization, methodology, writing–review and editing. **M.A. Dammert:** Formal analysis, validation, investigation, visualization, methodology. **C. Lorenz:** Formal analysis, investigation. **J. Brägelmann:** Investigation, visualization. **H.L. Tumbrink:** Investigation, visualization. **S. Klein:** Formal analysis, investigation. **A. Schmitt:** Investigation, methodology. **R. Büttner:** Resources. **T. Persigehl:** Resources. **K.M. Shokat:** Resources. **F. Wunderlich:** Conceptualization, resources, methodology. **A.M. Schram:** Writing–review and editing. **M. Peifer:** Resources, software. **M.L. Sos:** Conceptualization, resources, supervision, methodology. **H.C. Reinhardt:** Conceptualization, resources, supervision, methodology, writing–review and editing. **R.K. Thomas:** Conceptualization, resources, supervision, funding acquisition, methodology, project administration, writing–review and editing.

Acknowledgments

This work was supported by the German Ministry of Science and Education (BMBF) as part of the e:Med program (InCa, grant ID: 01ZX1901 to R.K. Thomas, H.C. Reinhardt, M.L. Sos, M. Peifer, F. Wunderlich, and L. Werr), the German Research Foundation (DFG, Deutsche Forschungsgemeinschaft) as part of SFB1399 (grant ID 413326622 to R.K. Thomas, H.C. Reinhard, M.L. Sos, R. Büttner, F. Wunderlich, M. Peifer, and J. Brägelmann), the German federal state North Rhine Westphalia (NRW) as part of the EFRE initiative (EFRE-0800397 to R.K. Thomas, M.L. Sos, and R. Büttner) and by the future concept of the University of Cologne as part of the Excellence Initiative (Max-Delbrück-Price to R.K. Thomas). This work was supported by the Köln Fortune program from L. Werr. D. Plenker was supported by the German Research Foundation (DFG, PL 894/1-1). J. Brägelmann was supported by the Else Kröner Fresenius Stiftung (Memorial Grant 2018_EKMS.35) and a Mildred Scheel Nachwuchszentrum Grant (70113307). This work was supported by NCI P30CA008748 CCITLA, Memorial Sloan Kettering Cancer Center Support Grant (P30 CA008748) to A. Schmitt. H.C. Reinhardt received funding through the German-Israeli Foundation for Research and Development (I-65-412.20-2016), the Deutsche Forschungsgemeinschaft (RE 2246/13-1), and the Deutsche Krebshilfe (1117240 and 70113041).

ROSA26:Flp knock in mice (Flp-deleter) were a kind gift from Susan M. Dymecki. The Ba/F3 ERBB2YF/ ERBB3 wt cells were a kind gift from Kevan M. Shokat. pBABE-hygro was a gift from Hartmut Land, Jay Morgenstern, and Bob Weinberg (Addgene plasmid No. 1765). We thank Alexandra Florin and Ursula Rommerscheidt-Fuß from the Institute of Pathology, University Hospital Cologne, for their technical support.

The costs of publication of this article were defrayed in part by the payment of page charges. This article must therefore be hereby marked *advertisement* in accordance with 18 U.S.C. Section 1734 solely to indicate this fact.

Received October 5, 2021; revised December 21, 2021; accepted February 15, 2022; published first February 28, 2022.

References

1. Fernandez-Cuesta L, Plenker D, Osada H, Sun R, Menon R, Leenders F, et al. CD74-NRG1 fusions in lung adenocarcinoma. Cancer Discov 2014;4:415–22.
2. Mei L, Xiong WC. Neuregulin 1 in neural development, synaptic plasticity and schizophrenia. Nat Rev Neurosci 2008;9:437–52.
3. Jonna S, Feldman RA, Swensen J, Gatalica Z, Korn WM, Borghaei H, et al. Detection of NRG1 gene fusions in solid tumors. Clin Cancer Res 2019;25:4966–72.
4. Ptakova N, Martinek P, Holubec L, Janovsky V, Vancurova J, Grossmann P, et al. Identification of tumors with NRG1 rearrangement, including a novel putative pathogenic UNC5D-NRG1 gene fusion in prostate cancer by data-drilling a de-identified tumor database. Genes Chromosomes Cancer 2021;60:474–81.
5. Heining C, Horak P, Uhrig S, Codo PL, Klink B, Hutter B, et al. NRG1 fusions in KRAS wild-type pancreatic cancer. Cancer Discov 2018;8:1087–95.
6. Dermawan JK, Zou Y, Antonescu CR. Neuregulin 1 (NRG1) fusion-positive high-grade spindle cell sarcoma: a distinct group of soft tissue tumors with metastatic potential. Genes Chromosomes Cancer 2021;61:123–30.
7. Jones MR, Lim H, Shen Y, Pleasance E, Ch'ng C, Reisle C, et al. Successful targeting of the NRG1 pathway indicates novel treatment strategy for metastatic cancer. Ann Oncol 2017;28:3092–7.
8. Jones MR, Williamson LM, Topham JT, Lee MKC, Goytain A, Ho J, et al. NRG1 gene fusions are recurrent, clinically actionable gene rearrangements in KRAS wild-type pancreatic ductal adenocarcinoma. Clin Cancer Res 2019;25:4674–81.
9. Odintsov I, Mattar MS, Lui AJW, Offin M, Kurzatkowski C, Delasos L, et al. Novel preclinical patient-derived lung cancer models reveal inhibition of HER3 and MTOR signaling as therapeutic strategies for NRG1 fusion-positive cancers. J Thorac Oncol 2021;16:1149-65.
10. Odintsov I, Lui AJW, Sisso WJ, Gladstone E, Liu Z, Delasos L, et al. The anti-HER3 mAb seribantumab effectively inhibits growth of patient-derived and isogenic cell line and xenograft models with oncogenic NRG1 fusions. Clin Cancer Res 2021;27:3154–66.
11. Murayama T, Nakaoku T, Enari M, Nishimura T, Tominaga K, Nakata A, et al. Oncogenic fusion gene CD74-NRG1 confers cancer stem cell-like properties in lung cancer through a IGF2 autocrine/paracrine circuit. Cancer Res 2016;76:974–83.
12. Gay ND, Wang Y, Beadling C, Warrick A, Neff T, Corless CL, et al. Durable response to afatinib in lung adenocarcinoma harboring NRG1 gene fusions. J Thorac Oncol 2017;12:e107–10.
13. Drilon A, Somwar R, Mangatt BP, Edgren H, Desmeules P, Ruusulehto A, et al. Response to ERBB3-directed targeted therapy in NRG1-rearranged cancers. Cancer Discov 2018;8:686–95.
14. Schram AM, Drilon AE, Macarulla T, O'Reilly EM, Rodon J, Wolpin BM, et al. A phase II basket study of MCLA-128, a bispecific antibody targeting the HER3 pathway, in NRG1 fusion-positive advanced solid tumors. J Clin Oncol 2020;38(15_suppl):TPS3654.
15. Schram AM. Efficacy and safety of zenocutuzumab in advanced pancreas cancer and other solid tumors harboring NRG1 fusions. In Proceedings of the American Society of Clinical Oncology (ASCO) 2021 Annual Meeting 2021.
16. Novotny CJ, Pollari S, Park JH, Lemmon MA, Shen W, Shokat KM. Overcoming resistance to HER2 inhibitors through state-specific kinase binding. Nat Chem Biol 2016;12:923–30.
17. Plenker D. Functional analysis of CD74-NRG1- a new recurrent oncogenic gene fusion in lung adenocarcinoma, in Mathematisch-Naturwissenschaftliche Fakultät. Universität zu Köln: Köln. 2015.

18. Bragelmann J, Dammert MA, Dietlein F, Heuckmann JM, Choidas A, Bohm S, et al. Systematic kinase inhibitor profiling identifies CDK9 as a synthetic lethal target in NUT midline carcinoma. Cell Rep 2017;20: 2833–45.
19. Bragelmann J, Lorenz C, Borchmann S, Nishii K, Wegner J, Meder L, et al. MAPK-pathway inhibition mediates inflammatory reprogramming and sensitizes tumors to targeted activation of innate immunity sensor RIG-I. Nat Commun 2021;12:5505.
20. Dobin A, Davis CA, Schlesinger F, Drenkow J, Zaleski C, Jha S, et al. STAR: ultrafast universal RNA-seq aligner. Bioinformatics 2013;29:15–21.
21. Li B, Dewey CN. RSEM: accurate transcript quantification from RNA-Seq data with or without a reference genome. BMC Bioinf 2011;12:323.
22. Love MI, Huber W, Anders S. Moderated estimation of fold change and dispersion for RNA-seq data with DESeq2. Genome Biol 2014;15:550.
23. Farley FW, Soriano P, Steffen LS, Dymecki SM. Widespread recombinase expression using FLPeR (flipper) mice. Genesis 2000;28:106–10.
24. Falls DL. Neuregulins: functions, forms, and signaling strategies. Exp Cell Res 2003;284:14–30.
25. Wilson TR, Fridlyand J, Yan Y, Penuel E, Burton L, Chan E, et al. Widespread potential for growth-factor-driven resistance to anticancer kinase inhibitors. Nature 2012;487:505–9.
26. Schaefer G, Fitzpatrick VD, Sliwkowski MX. Gamma-heregulin: a novel heregulin isoform that is an autocrine growth factor for the human breast cancer cell line, MDA-MB-175. Oncogene 1997;15:1385–94.